The Astrophysical Journal, 753:99 (10pp), 2012 July 10 doi:10.1088/0004-637X/753/2/99

SPECKLE NOISE SUBTRACTION AND SUPPRESSION WITH ADAPTIVE OPTICS CORONAGRAPHIC IMAGING

Deqing Ren[1,2,3], Jiangpei Dou[2,3], Xi Zhang[2,3,4], and Yongtian Zhu[2,3]
[1] Physics & Astronomy Department, California State University Northridge, CA 91330-8268, USA; ren.deqing@csun.edu
[2] National Astronomical Observatories/Nanjing Institute of Astronomical Optics & Technology, Chinese Academy of Sciences, Nanjing 210042, China
[3] Key Laboratory of Astronomical Optics & Technology, National Astronomical Observatories/Nanjing Institute of Astronomical Optics & Technology, Chinese Academy of Sciences, Nanjing 210042, China
[4] Graduate School of the Chinese Academy of Sciences, 19A Yuquanlu, Beijing 100049, China
Received 2011 December 6; accepted 2012 May 3; published 2012 June 18

ABSTRACT

Future ground-based direct imaging of exoplanets depends critically on high-contrast coronagraph and wave-front manipulation. A coronagraph is designed to remove most of the unaberrated starlight. Because of the wave-front error, which is inherit from the atmospheric turbulence from ground observations, a coronagraph cannot deliver its theoretical performance, and speckle noise will limit the high-contrast imaging performance. Recently, extreme adaptive optics, which can deliver an extremely high Strehl ratio, is being developed for such a challenging mission. In this publication, we show that barely taking a long-exposure image does not provide much gain for coronagraphic imaging with adaptive optics. We further discuss a speckle subtraction and suppression technique that fully takes advantage of the high contrast provided by the coronagraph, as well as the wave front corrected by the adaptive optics. This technique works well for coronagraphic imaging with conventional adaptive optics with a moderate Strehl ratio, as well as for extreme adaptive optics with a high Strehl ratio. We show how to substrate and suppress speckle noise efficiently up to the third order, which is critical for future ground-based high-contrast imaging. Numerical simulations are conducted to fully demonstrate this technique.

Key words: instrumentation: miscellaneous – planetary systems – techniques: high angular resolution – techniques: image processing

Online-only material: color figures

1. INTRODUCTION

Advances in past years using indirect imaging methods, such as measuring radial velocity and transiting light, infer that exoplanets may be common. Today, more than 700 exoplanets have been detected, of which only a few have been found by direct imaging. Future exoplanet discoveries with direct imaging will be one of the most important scientific advances in astronomy and will allow us to detect photons directly from exoplanets and use spectroscopy to analyze physical and atmospheric conditions. The development of such techniques will allow us to answer a key scientific question—Does another Earth exist in the universe? Such direct detection remains technologically challenging, since a very high contrast ratio and small angular separation are involved.

The few exoplanets found by direct imaging were imaged directly at a contrast of only 10^{-4} to 10^{-5}. These exoplanets are, in general, young and large and are still hot, which make them easy to be imaged in the infrared. An example is HR 8799, which has an age of 60 million years. The four orbiting planets of HR 8799 have an effective temperature between 870 and 1090 K and a mass between 5 and 7 M_J. They were initially detected by Marois et al. (2008, 2010), using a data reduction technique called angular differential imaging (Marois et al. 2006). The same exoplanets were also detected recently by using an adaptive optics (AO) coronagraph that delivers a contrast of less than 10^{-5} (Serabyn et al. 2010). The discovery of the HR 8799 exoplanets is a good example, and demonstrates the power of data reduction (Marois et al. 2008) and AO coronagraphic imaging (Serabyn et al. 2010). For ground-based observations, speckle noise will be the dominant limiting factor for high-contrast imaging. Speckle noise can be decomposed as different-order speckles of a polynomial expansion, in which each order or term of the speckle is relevant to the associated power of the pupil phase error. Speckle noise properties are discussed by many authors (Perrin et al. 2003; Bloemhof 2003, 2004, 2007) who focused on the suppression of the first-order speckle induced by the first power of the pupil phase error. For exoplanets with an age similar to our own planets, a higher contrast is required. Future ground-based coronagraphic imaging, coupled with extreme AO that can deliver an extremely high Strehl ratio, should be able to provide a contrast on the order of 10^{-7} (Thomas et al. 2011; Guyon et al. 2011; Patel & Metchev 2011; Stuik et al. 2010).

In this paper, we further extend the previous authors' work, and discuss a technique that fully takes advantage of the high contrast provided by the coronagraph and the wave front corrected by AO. The technique we used is based on image rotation and subtraction, in which the even-order and non-zero-mean speckles are subtracted, leaving odd-order and zero-mean speckles, which can be further suppressed by a high-contrast coronagraph and further reduced or averaged out by a long exposure with an AO-corrected image of a proper Strehl ratio. We show how to substrate and suppress the speckles efficiently up to the third order. In Section 2, we briefly review the speckle noise properties and provide a basic theory that will eventually lead to the subtraction and suppression of the speckle noise. In Section 3, we conduct numerical simulations to further demonstrate and verify the technique. The impact of the amplitude error is discussed in Section 4. Conclusions are presented in Section 5.

2. WAVE-FRONT ERROR PROPERTIES AND IMAGE ROTATION SUBTRACTION

The properties of speckle noise have been discussed by many authors (Racine et al. 1999; Sivaramakrishnan et al. 2002; Perrin et al. 2003; Bloemhof 2004, 2007; Ren & Wang 2006). In general, the pupil wave-front error or phase Φ of an electromagnetic wave can be expressed as a convergent Taylor series $e^{i\Phi} = 1 + i\Phi - \Phi^2/2 - i\Phi^3/6 + \Phi^4/24 + \ldots$. For a small Φ (in radian), a higher order power will have a smaller value than that of a lower order, and will in general contribute less to the speckle noise. A full expansion of the speckles for the aberrated point-spread function (PSF) intensity was discussed by Perrin et al. (2003). For a wave-front or phase error Φ and a normalized pupil function A, the focal plane PSF intensity distribution up to the fourth-order speckle was derived in our previous publication (Ren & Wang 2006), which is suitable for an unapodized pupil. A coronagraph can use an apodized pupil to attenuate the diffraction light from an aperture, so that high contrast is available in a discovery area. For a real pupil function A, the electric field strength is $Ae^{i\Phi}$ on the pupil, and the field strength on the focal plane is the Fourier transform of $Ae^{i\Phi}$. Truncating the above expansion above the fourth order, we provide the abberrated PSF intensity distribution that is suitable for both unapodized and apodized pupils as

$$I = (\overline{Ae^{i\Phi}}) \cdot (\overline{Ae^{i\Phi}})^* = |\bar{A}|^2 + n_1 + n_2 + n_3 + n_4, \quad (1)$$

where the over-line denotes a two-dimensional Fourier transform, and $*$ denotes a complex conjugate operation. $|\bar{A}|^2 = A \cdot A^*$ is the perfect PSF without a wave-front error, and is an even and real function. For simplicity, we assume that the pupil is symmetric (i.e., A is even). Therefore, $\bar{A}$ is real. n_2 and n_4 are the second order and fourth order of the speckles in the wave-front error, respectively. The terms $|\bar{A}|^2$, n_2, and n_4 are even and symmetric around the PSF center. Since we are only concerned with the odd-order speckles, which are anti-symmetric, we only provide explicit expressions for the odd-order speckles. The first-order and third-order speckles are given as

$$n_1 = \bar{A}[2\mathrm{Im}(\overline{\Phi A}^*)], \quad (2)$$

$$n_3 = \mathrm{Im}[\overline{\Phi A}(\overline{\Phi^2 A}^*)], \quad (3)$$

where Im denotes the imaginary part of a complex. Here, we have omitted the term $-\mathrm{Im}[\bar{A}(\overline{\Phi^3 A}^*)]/3$ in the third-order speckle, since this term can be efficiently suppressed by a high-contrast coronagraph (i.e., suppressed by $\bar{A}$) and is less dominant. Being spatially anti-symmetric, the odd-order speckles n_1 and n_3 have negative and positive values as well as a zero mean at any focal plane position for a long exposure image. In the case that the static wave-front aberration is corrected with an extreme AO system, the residual wave-front error Φ will be randomly changed since the incoming atmospheric turbulence-induced wave-front error is randomly variable. Because they can be negative and positive on any spatial position on the focal plane for each short-exposure image that typically has an exposure time equal to the speckle life, they could, in principle, be averaged out to zero by co-adding infinite short-exposure images, or be significantly reduced by co-adding a large number of short-exposure images. The even-order speckles have a positive value and cannot be averaged out by co-adding short-exposure images, which will reduce the dynamic range for high-contrast coronagraphic imaging. Because of the symmetry, all the even-order speckles, including the perfect PSF $|\bar{A}|^2$, can be eliminated by subtracting a copy of the original image with a 180° rotation around the PSF center. For such a co-subtracted image, one has

$$n_{\mathrm{sub}} = n_1 + n_3. \quad (4)$$

Please note that the overall PSF intensity I of an image in Equation (1) is always positive (or zero). In the real world, the speckles cannot exist independently. However, they can be isolated by manipulating the images. For example, the subtraction of an image with its rotation copy can result in a positive or negative value depending on local relative intensity values of the two images, which gives the sum of all the odd-order speckles. For the same reason, an odd-order speckle can be negative or positive, which is determined by its expression, and the properties of the first-order speckle were well discussed by Bloemhof (2003).

After the image rotation subtraction, only odd-order speckles are left. Therefore, for high-contrast imaging with the image rotation subtraction, the contrast can be improved, if the odd-order speckles were suppressed. For a moderate or high Strehl ratio, the wave-front or phase error Φ (in the unit of radian) is much less than 1. A higher-order power of phase error Φ will be less than a lower-order power, and this is also true for its Fourier transform and the conjugate of the Fourier transform. Therefore, low-order speckles will in general be dominant. This is demonstrated in the next section, in which the same phase map (in the unit of nanometer) is scaled with a wavelength, giving different wave-front errors with different Strehl ratios.

Please note that the boundary of Φ is defined by the unapodized pupil (i.e., the circular telescope aperture). Φ is zero only outside the unapodized pupil. For an unapodized pupil, we have $\Phi A = \Phi$ and $\Phi^2 A = \Phi^2$. Also $\bar{A}$ is real for a symmetric pupil. For an unapodized pupil (i.e., without a coronagraph), Equations (2) and (3) for the odd-order speckles can be simplified as

$$n_1' = \bar{A}[2\mathrm{Im}(\bar{\Phi}^*)], \quad (5)$$

$$n_3' = \mathrm{Im}[\bar{\Phi}(\bar{\Phi}^{2*})]. \quad (6)$$

This well-known speckle n_1' is discussed by many authors (Perrin et al. 2003; Bloemhof 2004, 2007; Ren & Wang 2006). Since the wave-front error (i.e., $[2\mathrm{Im}(\bar{\Phi}^*)]$) is attenuated by $\bar{A}$ of the square root of the perfect PSF, the first-order speckle is pinned to the star's diffraction pattern (Bloemhof 2004). The third-order speckle n_3' has not been discussed, since it is believed that the first-order speckle n_1' is dominant. This is generally true for an unapodized pupil. At the angular distance 5 λ/D from the perfect PSF center, which is in an interesting area for high-contrast imaging, the perfect unapodized PSF $|\bar{A}|^2$ provides a contrast of 10^{-3} and the real number $\bar{A}$ has a value of $\sim 3 \times 10^{-2}$. Therefore, the first-order speckle is suppressed $1/(3 \times 10^{-2})$ times by a circular unapodized aperture. It is very interesting that the third-order speckle of Equation (6) is a function of Φ only, and therefore, it can only be suppressed by reducing the wave-front error. Although the analysis is done by using an unapodized pupil, it can also be applied to an apodized pupil, and the only difference is that the third-order speckle may become dominant with an apodized pupil, if the first-order speckle is efficiently suppressed.

The first-order speckle can be efficiently suppressed by an apodized pupil. Comparing Equations (2) and (5), the term

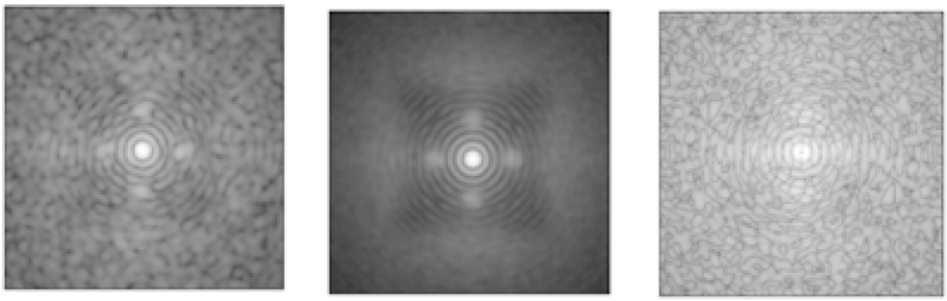

Figure 1. PSFs without a coronagraph with a 0.57 Strehl ratio. Left: four-image PSF; center: 100 image PSF; right: 100 image residual PSF after image rotation subtraction.

$[2\mathrm{Im}(\bar{\Phi}^*)]$ for an unapodized pupil is replaced by $[2\mathrm{Im}(\overline{\Phi A}^*)]$ for an apodized pupil. This term can be further expressed as $[2\mathrm{Im}(\bar{\Phi} \otimes \bar{A})^*]$. Since $|\bar{A}|^2$ is a "star-like" normalized function, $\bar{A}$ is also a "star-like" normalized function. The convolution of $\bar{\Phi}$ with a "star-like" normalized function $\bar{A}$ only slightly "broadens" or "blurs" the distribution of $\bar{\Phi}$, which only reduces its "spatial resolution" and will not affect the local speckle too much. This is very similar to the convolution of a perfect two-dimensional scene with an aberrated PSF induced by the optics aberrations of an imaging system, in which the scene (here it is $\bar{\Phi}$) will be blurred by the PSF (here it is $\bar{A}$), which reduces the spatial resolution and results in a local intensity average. Therefore, there is little difference between $[2\mathrm{Im}(\bar{\Phi}^*)]$ and $[2\mathrm{Im}(\overline{\Phi A}^*)]$, in view of the speckle value. For a coronagraph that is designed to deliver a contrast of 10^{-5}, for example, the $\bar{A}$ will have a value on the order of 3×10^{-3} in the discovery area, and the first-order speckle will be suppressed 10 times better than that of the unapodized pupil. These discussions can also be applied to the third-order speckle $\mathrm{Im}[\overline{\Phi A}(\overline{\Phi^2 A}^*)]$, which can be approximated as $\mathrm{Im}[\bar{\Phi}(\bar{\Phi}^{2*})]$. Therefore, the analysis for the non-apodized pupil can be applied to the apodized pupil.

When a high-contrast coronagraph is used, the term $\bar{A}$ will have a small value in the coronagraph's optimized discovery area. Thus the first-order speckle can be efficiently attenuated, which may lead the third-order speckle to be dominant, since the third-order speckle is almost independent to the pupil function A and is mainly determined by the wave-front error. In the case where the first-order speckle is efficiently suppressed, continuing increasing the coronagraph theoretical contrast will not help to further suppress the speckle noise, and the contrast can only be improved by increasing the Strehl ratio or/and increasing the image exposure time. Understanding these factors is important for the design of future high-contrast coronagraphs.

Since for co-added images the odd-order speckles have zero mean at any position on the focal plane, they can be averaged to a small value for an image with a long exposure time, even though the AO system has a moderate Strehl ratio. This requires that the static aberration of the AO system must be corrected or the AO system must be well calibrated by an appropriate technique, which is in general required by an extreme AO system (Sauvage et al. 2007). If we assume that the speckle life is τ, for an image with exposure time T, the odd-order speckles will be reduced by $\sqrt{T/\tau}$ times compared with that of an exposure τ. Therefore, the contrast will have an extra gain of $\sqrt{T/\tau}$ times better.

3. NUMERICAL SIMULATIONS

The AO system that we used for the numerical simulations has a deformable mirror (DM) with 20×20 actuators and a Shark–Hartmann wave-front sensor with 24×24 sub-apertures. The telescope is assumed to have a 3 m circular aperture without a central obstruction. The small telescope aperture can deliver an acceptable imaging performance at the visible, with a moderate DM actuator number. The open-loop correction frequency is 1000 Hz. The Fried parameter r_0 is 80 mm at 500 nm, which corresponds to a seeing condition of $1\farcs3$. The software package CAOS, which is developed by a number of European institutions, is used to generate the AO-corrected phase maps. For simplicity, no photon and read-out noise is included. We assume that the AO non-common optical path error that is induced by the differential optical paths between the wave-front sensor and science camera is fully corrected by an appropriate technique (Ren et al. 2012).

The high-contrast coronagraph that we used for this simulation is based on the transmission apodizing pupil (Ren & Zhu 2007), which can be designed to provide a theoretical contrast up to 10^{-10}, and it is delivering a contrast close to 10^{-7} in the laboratory for a circular aperture with a central obstruction (Ren et al. 2010). The simulation results from the transmission apodizing pupil will, in general, also hold true for other types of coronagraphs.

We generate 100 independent AO-corrected phase maps. Each phase map is taken in a de-correlation timescale equal to the speckle life. Each PSF is then calculated according to the associated phase map. Thus, each PSF can be viewed to be taken with a short exposure time that is equal to the speckle life. For the above AO system, the RMS residual phase error is 95 nm on average, with a few nanometer differences in each phase map. Each phase map is scaled to be exactly equal to 95 nm, so that comparisons that involve the PSF number will be accurate. According to Macintosh et al. (2005), the speckle life is irrespective of Fried parameter r_0 or the AO system, and is given as $0.6\,D/v$, where D is the telescope aperture diameter and v is the wind speed. For a 3 m telescope with a wind speed of 8 m s^{-1}, the speckle life is 0.225 s and an exposure of 5 hr corresponds to 80,000 de-correlation images.

In our simulations, Strehl ratios with different values are achieved by shifting the wavelength. The 95 nm phase error corresponds to a Strehl ratio of 0.57 and 0.88 at the wavelengths $0.8\,\mu$m and $1.65\,\mu$m, respectively. Figure 1 shows the PSFs, and the residual PSF after image rotation subtraction, with 0.57 Strehl ratio at the $0.8\,\mu$m wavelength, respectively. The left panel shows the co-added PSF of four images, while the co-added PSF of 100 images is shown in the central panel. The co-added PSF of the 100 images is rotated by 180° and is subtracted with its original PSF of 100 co-added images, with the residual PSF after the image rotation subtraction shown in the right panel. The subtracted PSF is shown as an absolute value only, although the subtraction may result in positive and negative values, and

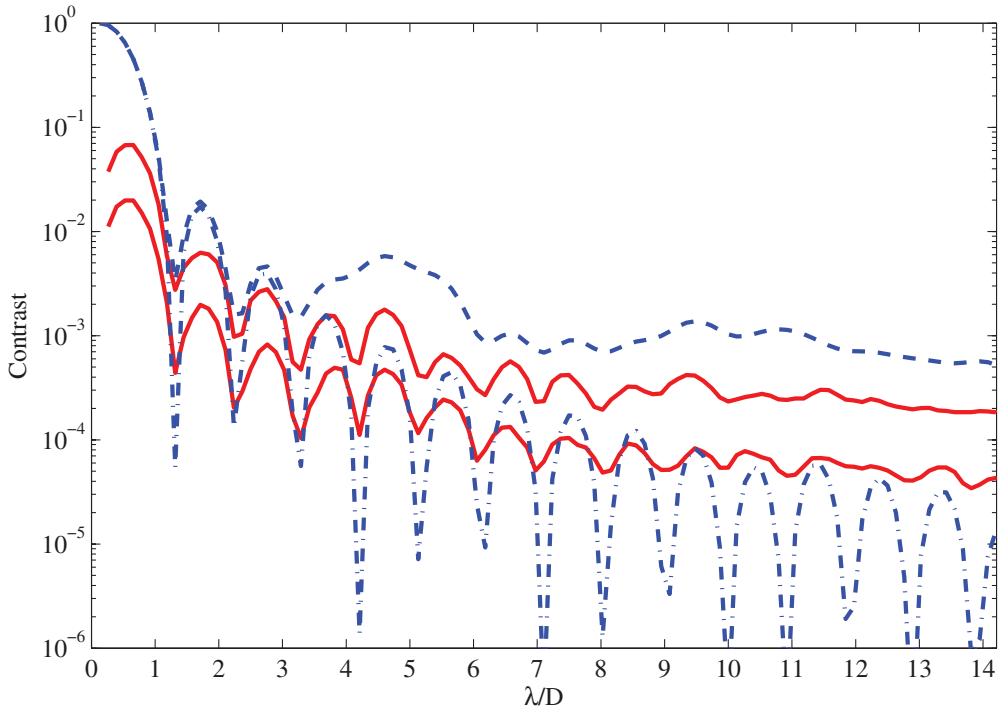

Figure 2. Contrasts without a coronagraph with a 0.57 Strehl ratio. Dashed line: 100 image contrast; dash-dotted line: theoretical contrast; top solid line: four-image residual contrast after image rotation subtraction; bottom solid line: 100 image residual contrast after image rotation subtraction.

(A color version of this figure is available in the online journal.)

has a zero mean for a long-exposure image. For a speckle life of 0.225 s, the four-image PSF corresponds to an exposure of 0.9 s, while the 100 image PSF corresponds to that of 2.25 s. The dark square pattern and the four spots in the left and center panels resulted from the diffraction that is inherited from the grid arrangement of the DM actuators. This aperture diffraction pattern stands out and is more dominant when the exposure time increases or more images are co-added, which is clearly indicated from the comparison of the left and center panels. Figure 2 shows the corresponding annulus-average contrasts and residual contrast after the image rotation subtraction. The dashed line is the contrast of the PSF of 100 co-added images. The bottom solid line is the residual contrast of the PSF of the 100 co-added images after the image rotation subtraction, where the residual contrast after the image rotation subtraction is defined as the subtracted residual intensity normalized by the peak intensity before the subtraction. It is clear that the image rotation subtraction technique dramatically improves the contrast, and an extra contrast gain of more than 10 times is achieved for the 100 co-added images after the image rotation subtraction. The top solid line shows the residual contrast of four co-added images after the image rotation subtraction applied. The two solid lines pin very well with the theoretical diffraction pattern (dash-dotted line) of the circular aperture, indicating that the first-order speckle dominates the contrast performance. Comparing the two solid lines with the image rotation subtraction, the 100 co-added images after the image rotation subtraction provides an extra five-time contrast improvement over that of the four co-added images, which is exactly equal to $\sqrt{100/4}$, as estimated. The contrast is improved as the squared root of the de-correlation image number. The contrast of the 100 co-added images without any data reduction (dashed line) cannot be better than that of the theoretical contrast (dash-dotted line). It is also clear that given a proper exposure time, the residual contrast with image rotation subtraction can be easily superior to the theoretical contrast determined by diffraction only. Therefore, simply increasing the exposure time without image subtraction has a very limited contrast performance that can never be better than the theoretical contrast, even though the wave-front error is reduced to an extreme small value. The contrast of the directly co-added images will be equal to that of the theoretical value only when the wave front is zero. The image rotation subtraction can provide an unlimited contrast improvement and provide a residual contrast better than the theoretical value, given that the exposure time is long enough.

Figure 3 is identical to Figure 2, except that the Strehl ratio is 0.88, which corresponds to the 1.65 μm wavelength for the same phase error of 95 nm. The same set of 100 phase maps is used. It is not surprising that the contrast of the 100 directly co-added images (dashed line) is still worse than that of the theoretical value (dash-dotted line), although there has been some improvement over that in Figure 1 because of the better Strehl ratio. Compared with the residual contrast of four co-added images (top solid line) after the image rotation subtraction, the contrast for the 100 co-added images (bottom solid line) after the image rotation is improved by $\sim$5 times, which is the same with that in Figure 2 and is as estimated. Again, the residual PSFs after the image rotation subtraction are pinned well with that of the theoretical diffraction pattern, indicating that the first-order speckle is still the dominant speckle noise that limits the contrast performance, even with a better Strehl ratio. It is clear that the residual contrast of the 100 co-added images after image rotation subtraction is better than that of the theoretical diffraction, which is an important feature for the image rotation subtraction technique.

Even though the image rotation subtraction technique can significantly improve the contrast, its performance is still limited by the first-order speckle for an unapodized pupil. The first-order speckle can be efficiently suppressed by using a

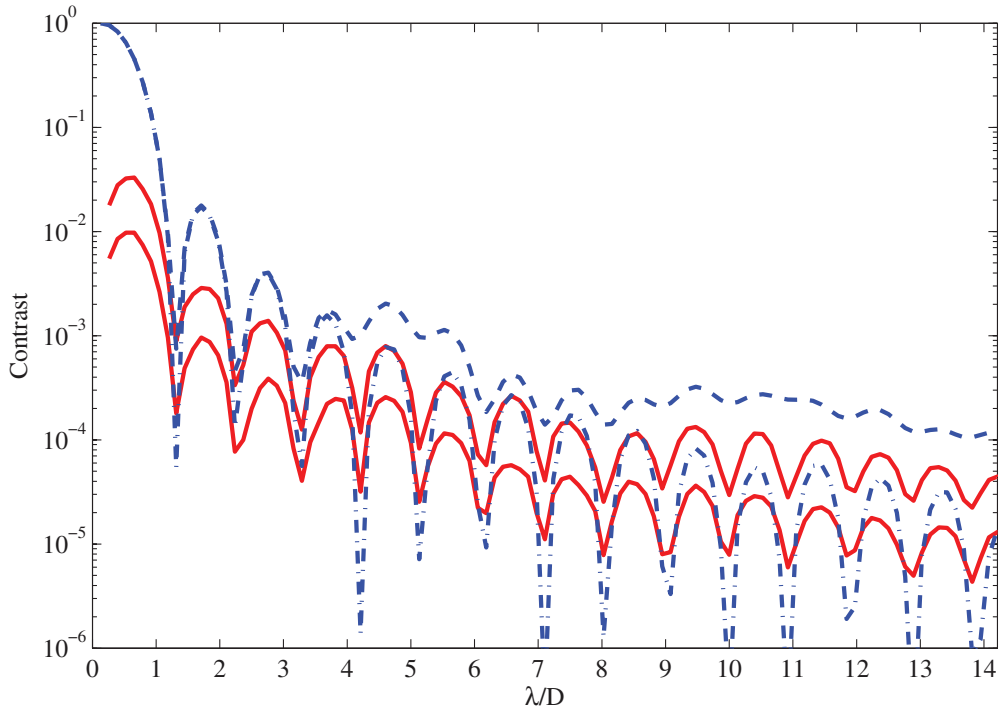

Figure 3. Contrasts without a coronagraph with a 0.88 Strehl ratio. Dashed line: 100 image contrast; dash-dotted line: theoretical contrast; top solid line: four-image residual contrast after image rotation subtraction; bottom solid line: 100 image residual contrast after image rotation subtraction.
(A color version of this figure is available in the online journal.)

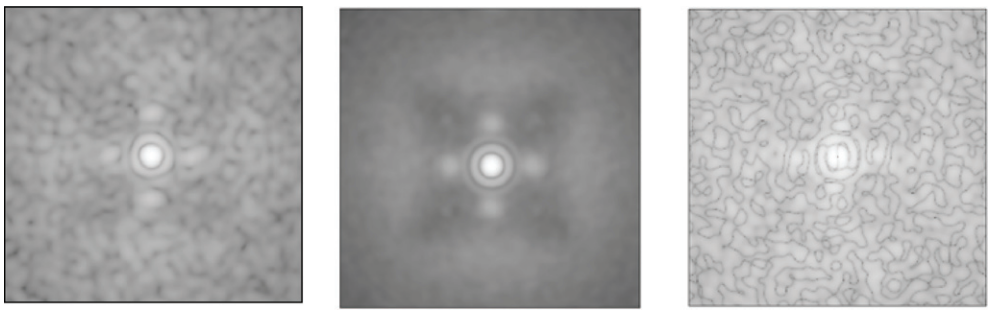

Figure 4. PSFs with a 10^{-5} coronagraph and 0.57 Strehl ratio. Left: four-image PSF; center: 100 image PSF; right: 100 image residual PSF after image rotation subtract.

coronagraph. Figure 4 shows the PSFs, and residual PSF after image rotation subtraction with a 0.57 Strehl ratio, which is identical to Figure 1 except that a coronagraph is used. The coronagraph is designed to provide a theoretical contrast of 10^{-5} in the discovery area at an angular distance larger than 4 λ/D in the ideal situation (without a wave-front error). Now, the circle aperture diffraction pattern of Figure 1 is hard to see since it is suppressed by the coronagraph. The corresponding contrasts and residual contrasts are shown in Figure 5, respectively. Comparing the dashed lines in Figures 2 and 5, a coronagraph contributes almost no extra contrast improvement in the case of a smaller Strehl ratio for the coronagraphic direct exposure PSF without image rotation subtraction. However, using the image rotation subtraction technique, a coronagraph can provide an extra contrast gain, even in the situation of a moderate Strehl ratio. At the closed angular distance around 5–6 λ/D, with the image rotation subtraction, the coronagraph suppresses the diffraction more efficiently and provides an extra residual contrast gain around 8 times compared with that without the coronagraph, which is close to our estimation of 10 times. At a large angle distance, there is no obvious difference with or without the coronagraph since the aperture diffraction is very low there and the coronagraph is not designed to suppress the diffraction at a large angular distance.

The coronagraph's performance can be further improved with a better wave-front correction. Figure 6 shows the contrasts and residual contrast with the 0.88 Strehl ratio at 1.65 μm wavelength, respectively. Compared with the residual contrast of the four co-added images (top solid line) after the image rotation, the residual contrast of the 100 co-added images (bottom solid line) after the image rotation subtraction is improved by $\sim$5 times, as estimated. The residual contrasts are stably improved with a better Strehl ratio. The two solid lines pin very well with the coronagraph's theoretical contrast (dash-dotted line), indicating that the first-order speckle is still dominant. The contrast of the 100 co-added images after the image rotation subtraction is close to its theoretical value, and a 5 hr exposure should provide a contrast close to 10^{-6}, which is better than that of the coronagraph's theoretical contrast.

Continuing to increase the coronagraph's theoretical contrast does not provide much contrast improvement if the Strehl ratio is not improved accordingly. Figure 7 shows the contrasts and

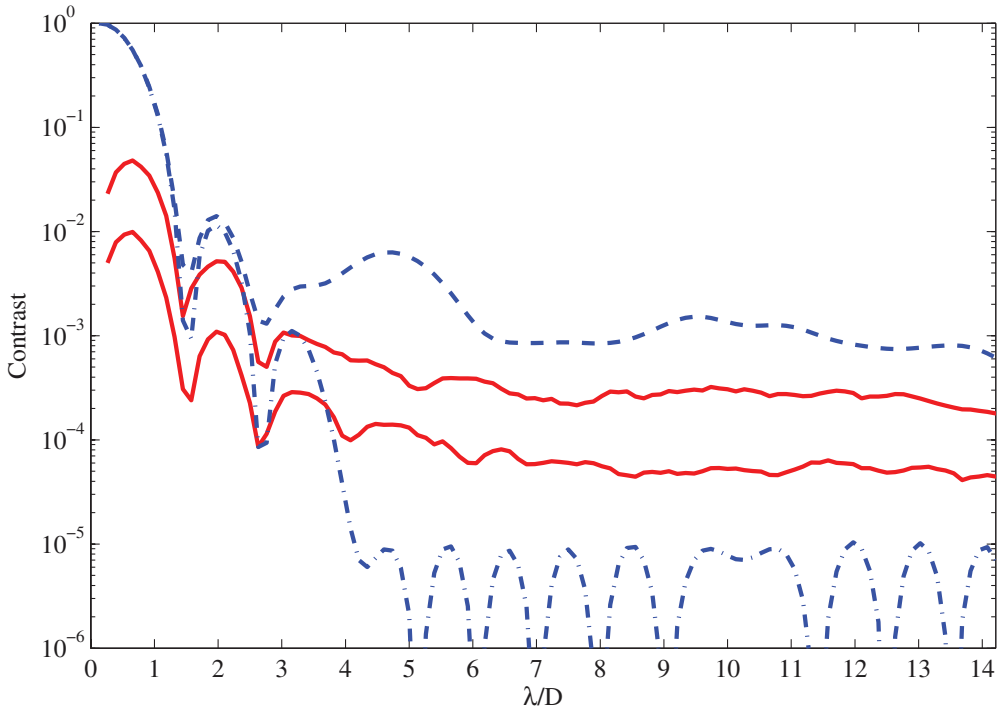

Figure 5. Contrasts with a 10^{-5} contrast coronagraph and 0.57 Strehl ratio. Dashed line: 100 image contrast; dash-dotted line: theoretical contrast; top solid line: four-image residual contrast after image rotation subtraction; bottom solid line: 100 image residual contrast after image rotation subtraction.
(A color version of this figure is available in the online journal.)

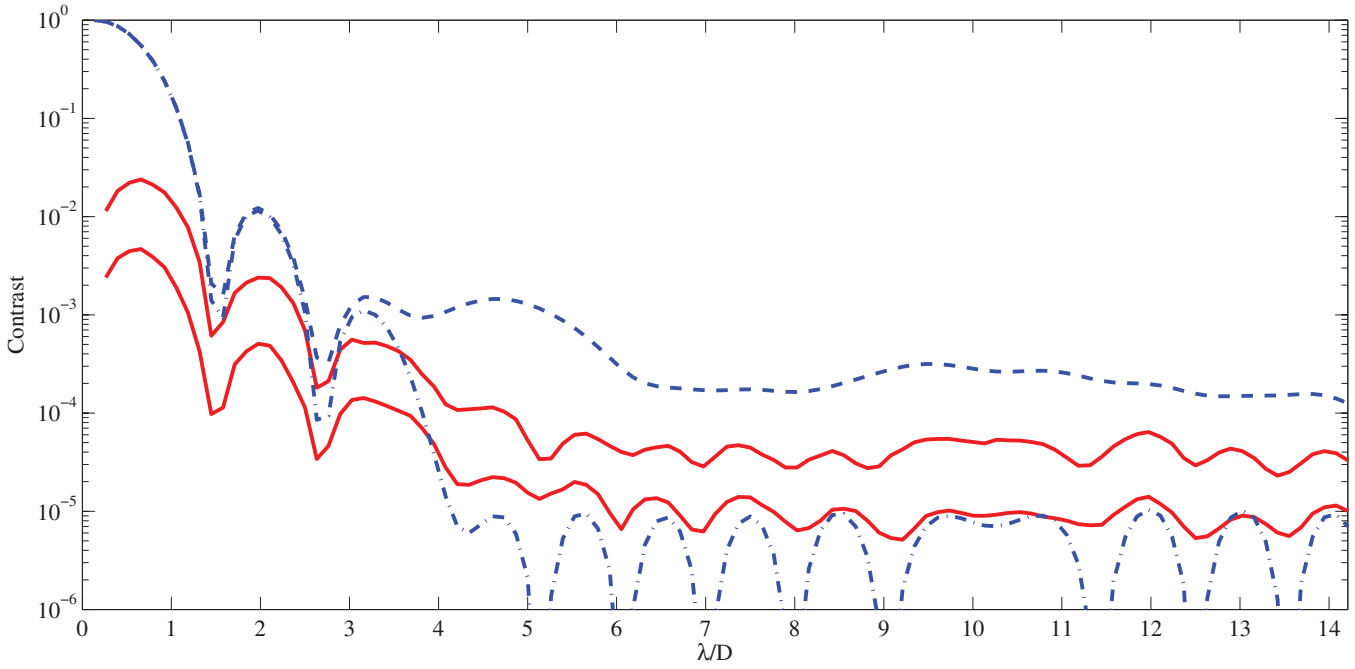

Figure 6. Contrasts with a 10^{-5} contrast coronagraph and 0.88 Strehl ratio. Dashed line: 100 image contrast; dash-dotted line: theoretical contrast; top solid line: four-image residual contrast after image rotation subtraction; bottom solid line: 100 image residual contrast after image rotation subtraction.
(A color version of this figure is available in the online journal.)

residual contrast in the same situation as that of Figure 6, except that the coronagraph has a theoretical contrast of 10^{-7}. It is clear that the two solid lines do not pin well with the coronagraph's theoretical contrast (dash-dotted line), indicating that the first-order speckle is not dominant. There is no significant residual contrast improvement compared with that in Figure 6 where the coronagraph has a theoretical contrast of 10^{-5}. This is because the first-order speckle is already efficiently suppressed and the speckle noise is dominated by the third-order speckle, which is almost independent to the coronagraph's theoretical contrast and is mainly determined by the wave-front error. In this case, the contrast can only be improved by reducing the wave-front error.

Figure 8 shows the contrasts and residual contrast at the 0.88 and 0.973 Strehl ratios for the 100 co-added images,

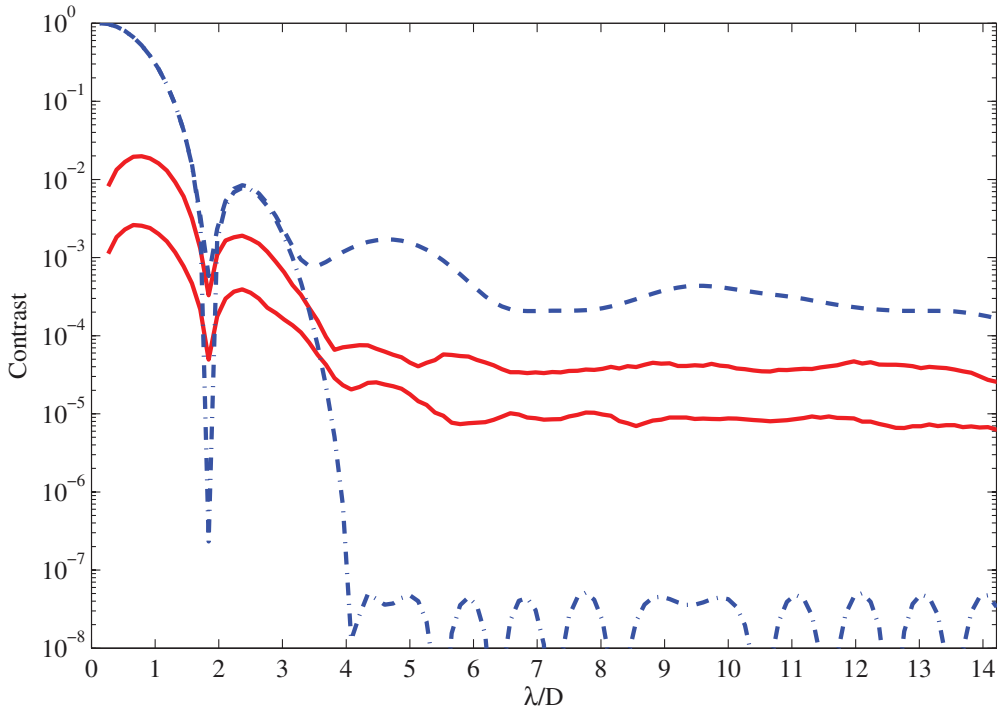

Figure 7. Contrasts with a 10^{-7} contrast coronagraph and 0.88 Strehl ratio. Dashed line: 100 image contrast; dash-dotted line: theoretical contrast; top solid line: four-image residual contrast after image rotation subtraction; bottom solid line: 100 image residual contrast after image rotation subtraction.
(A color version of this figure is available in the online journal.)

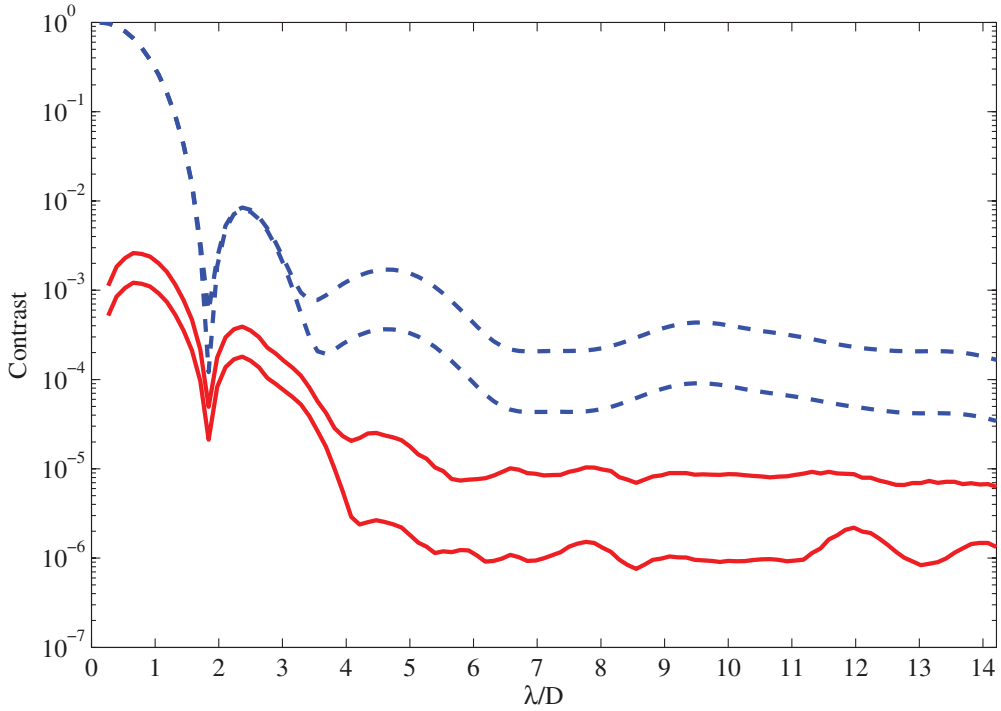

Figure 8. Contrasts without (top dashed line) image rotation subtraction and residual contrast (top solid line) after image rotation subtraction at 0.88 Strehl ratios; contrasts without (bottom dashed line) image rotation subtraction and residual contrast (bottom solid line) after image rotation subtraction at 0.97 Strehl ratios.
(A color version of this figure is available in the online journal.)

respectively. The wave fronts at the 0.973 Strehl ratio are simply scaled from that at 0.88. The coronagraph has a theoretical contrast of 10^{-7} at an angular distance larger than 4 λ/D. Since the first-order speckle is efficiently suppressed by the coronagraph in this case, the residual contrast is dominated by the third-order speckle that is mainly determined by the wave-front error. The RMS wave-front error is 0.357 and 0.166 rad at the 0.88 and 0.973 Strehl ratios, respectively. The contrast should be 10 times different, if the speckles are dominated by the third order, which is confirmed by our simulation in Figure 8,

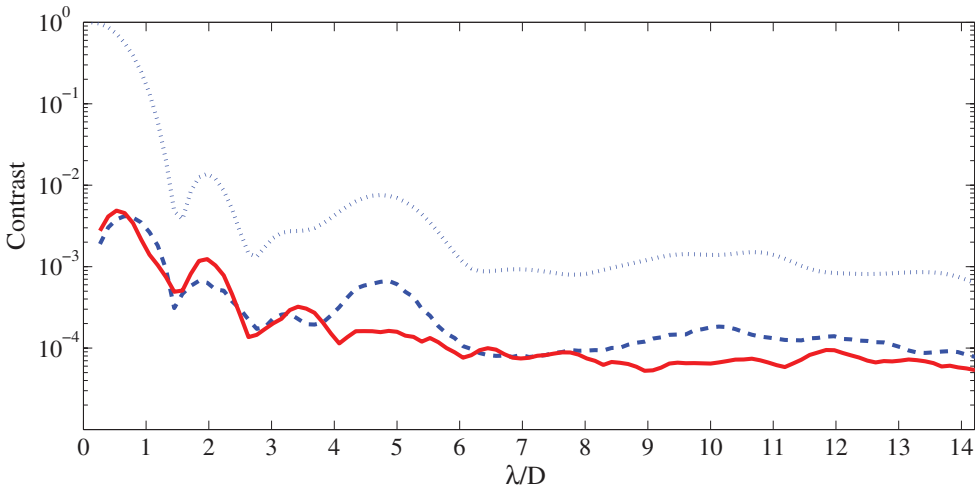

Figure 9. Contrast with a 10^{-5} contrast coronagraph at a 0.88 Strehl ratio. Dotted line: 50 image contrast; dashed line: residual contrast after reference star subtraction; solid line: residual contrast after image rotation subtraction.

(A color version of this figure is available in the online journal.)

in which the two solid lines of the 100 co-added images with the image rotation subtraction obey this rule very well in the discovery area for an angular distance larger than 4 λ/D. Also the residual contrast of 100 co-added images after image rotation subtraction at the 0.973 Strehl ratio is close to 10^{-6}, indicating that a 5 hr exposure image can deliver a residual contrast of 10^{-7}. For the 100 co-added images, the contrasts without image subtraction (dashed lines) can only provide a contrast worse than 10^{-3} and 10^{-4} for the 0.88 and 0.973 Strehl ratios, respectively, while the image rotation subtraction residual PSFs provided a residual contrast that is 100 times better and can be further improved by increasing the exposure time.

Finally, we compare the image rotation subtraction with the conventional reference star subtraction. We use a set of 50 short-exposure images to simulate the target star, and the other set of 50 images to simulate a reference star. The 50 images for the target star are co-added or summed to simulate a long-exposure target master image, and is applied with the image rotation subtraction. The 50 images for the reference star are also co-added to form a reference master image. The target master image is subtracted by the reference master image, which gives a conventional reference star subtraction image. Figure 9 shows the residual contrasts after the reference-star subtraction (dashed line) and the image rotation subtraction (solid line), as well as the contrast of the original target master image (dotted line) without any subtraction, with a coronagraph optimized for 10^{-5} theoretical contrast at an angular distance larger than 4 λ/D at the 0.88 moderate Strehl ratio. Compared with the original target master image (dotted line) without any data reduction, the reference star subtraction (dashed line) provides an extra contrast gain, indicating that the reference star subtraction is a useful approach. Please note that the area corresponding to the angular distance less than 4 λ/D is not a discovery area for the coronagraph and will not be evaluated (see the dash-dotted line in Figure 5 for the coronagraph's theoretical contrast). However in the coronagraph's optimized area with an angular distance larger than 4 λ/D, the image rotation subtraction is more powerful than the reference-star subtraction and delivers a better residual contrast than that of the reference-star subtraction. While the reference-star subtraction is more likely to bind to the original master target image (dotted line), the image rotation subtraction is less bound to it and is able to prove a clean and smooth subtraction with better residual contrast. In the coronagraph's optimized discovery area with an angular distance large than 4 λ/D, the residual contrast of the image rotation subtraction is in general superior to that of the reference star subtraction. This is because the even-order speckles cannot be effectively subtracted by reference star subtraction, while they can be totally subtracted by image rotation subtraction.

4. AMPLITUDE ERROR

In the previous discussions, we have not considered the possible amplitude error. For ground-based observations, the intensity over the telescope is variable from time to time because of the scintillation. This intensity variation induced amplitude error will degrade the actual coronagraphic performance. In the presence of the amplitude error, our image rotation subtraction technique will still be superior to the conventional reference star subtraction discussed, and the results that we have reached will still hold true as we discuss in this section. That is, the residual contrast with image rotation subtraction can be improved by increasing the exposure time.

In the presence of amplitude error, at any moment the actual pupil function A can be split as $A = A_0 + A_e$, where A_0 and A_e are the static theoretical pupil function and the dynamic zero mean pupil function errors, respectively (we note that A_e is real).

Scintillation creates additional odd speckles not removed by the rotation subtraction technique, but these speckles are fainter than the dominant even speckles (removed by our technique) and can be averaged down in long exposures.

Since both amplitude and wave-front errors are presented, the amplitude error modifies the pupil function A. The pure diffraction PSF of $|A_0|^2$ as well as all other even speckles can still be subtracted by image rotation subtraction. The remaining residual starlight is still only determined by the odd-term speckles, which can be further suppressed by increasing the exposure time exactly as there is no amplitude error except that the pupil function is somewhat modified by the amplitude error. To demonstrate this, we add a 3% rms intensity error in our simulation in which the coronagraph perfect pupil function A_0 is designed for a 10^{-5} contrast. The exact simulation of the scintillation-induced intensity distribution is complicated and not necessary here. We assume that the intensity is variable with a coherent size of r_0, the same as that of the Fried

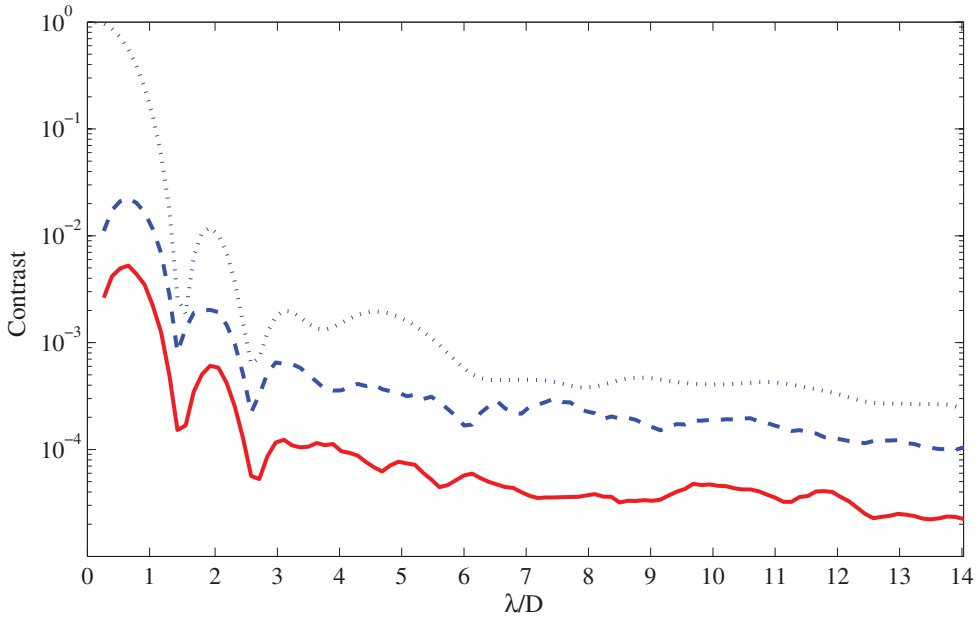

Figure 10. Contrasts with a 10^{-5} contrast coronagraph at a 0.88 Strehl ratio when both wave-front and amplitude errors are presented. Dotted line: 100 image contrast; dashed line: four-image residual contrast after image rotation subtraction; solid line: 100 image residual contrast after image rotation subtraction.
(A color version of this figure is available in the online journal.)

parameter at 0.8 μm. That is, there are about 24 intensity spatial elements across the pupil for a 3 m telescope. These low and medium frequencies of the intensity variation on the pupil greatly degrade the coronagraph's performance, compared with a higher frequency. The intensity is then converted to the amplitude error and added in the pupil function A, in which the amplitude error is randomly generated for each instant image. The wave-front error is also randomly added in each image, which corresponds to a Strehl ratio of 0.88, with the result shown in Figure 10. Comparing the residual contrasts of the four images and 100 images after image rotation subtraction, it is clear that the amplitude error degrades the coronagraph's contrast as estimated, since A is modified by the amplitude error induced by the scintillation. Image rotation subtraction will calibrate/remove speckles due to phase errors and can therefore work down to the scintillation limit at an approximately 10^{-5} contrast level on an 8 m telescope. Beyond this contrast level, because of the low contrast induced by the amplitude error, only time averaging from long exposure can further mitigate speckle noise.

5. CONCLUSIONS

The fact that speckle noise can be decomposed as different orders in respect to the wave-front error provides an opportunity to subtract and suppress the speckle noise. We have demonstrated the subtraction and suppression of speckles up to the third order. The even-order speckles can be subtracted by using the image rotation subtraction technique, leaving the odd-order speckles uncorrected. Without a high-contrast coronagraph, the first-order speckle can only be suppressed by increasing the exposure time, which provides a limited performance for high-contrast imaging leaving the first-order speckle dominant. The first-order speckle can be efficiently suppressed by using a high-contrast coronagraph, leaving the third-order speckle dominant, which is almost independent of the coronagraph's theoretical contrast. In the case that the first-order speckle is efficiently suppressed, continuing to increase the coronagraph's theoretical contrast will not help to further suppress the speckle noise, and the residual contrast with image rotation subtraction can only be improved with a better wave-front correction as well as increasing the exposure time. Given a long exposure time, the image rotation subtraction can provide a residual contrast better than that of the theoretical value. This also holds true for the situation when both wave-front and amplitude errors are presented. According to our knowledge, this is the first discussion that speckles up to third order can be suppressed by a proper combination of a high-contrast coronagraph and AO, and this work will be helpful to future coronagraph designs, as well as high-contrast imaging observations.

We thank the anonymous referee for valuable comments and careful corrections, which significantly improved the manuscript. This work is supported by the National Science Foundation under the grant ATM-0841440, the National Natural Science Foundation of China (NSFC) (Grants 10873024 and 11003031), and the National Astronomical Observatories' Special Fund for Astronomy-2009, as well as the Strategic Priority Research Program" of the Chinese Academy of Sciences (grant no. XDA04070600).

REFERENCES

Bloemhof, E. E. 2003, ApJ, 582, L59
Bloemhof, E. E. 2004, ApJ, 610, L69
Bloemhof, E. E. 2007, Opt. Exp., 15, 4705
Guyon, O., Martinache, F., Clergeon, C., et al. 2011, Proc. SPIE, 8149, 814908
Macintosh, B., Poyneer, L., Sivaramakrishnan, A., & Marois, C. 2005, Proc. SPIE, 5903, 170
Marois, C., Lafrenière, D., Doyon, R., Macintosh, B., & Nadeau, D. 2006, ApJ, 641, 556
Marois, C., Macintosh, B., Barman, T., et al. 2008, Science, 322, 1348
Marois, C., Zuckerman, B., Konopacky, Q. M., Macintosh, B., & Barman, T. 2010, Nature, 468, 1080
Patel, R., & Metchev, S. 2011, BAAS, 43, 128.02
Perrin, M. D., Sivaramakrishnan, A., Makidon, R. B., Oppenheimer, B. R., & Graham, J. R. 2003, ApJ, 596, 702
Racine, R., Walker, G. A. H., Nadeau, D., Doyon, R., & Marois, C. 1999, PASP, 111, 587
Ren, D., Dong, D., & Zhu, Y. 2012, PASP, 124, 247

Ren, D., Dou, J., & Zhu, Y. 2010, PASP, 122, 590
Ren, D., & Wang, H. 2006, ApJ, 640, 530
Ren, D., & Zhu, Y. 2007, PASP, 119, 1063
Sauvage, F., Fusco, T., Roussel, G., & Petit, C. 2007, J. Opt. Soc. Am. A, 24, 2334
Serabyn, E., Mawet, D., & Burruss, R. 2010, Nature, 464, 1018
Sivaramakrishnan, A., Lloyd, J. P., Hodge, P. E., & Macintosh, B. A. 2002, ApJ, 581, L59
Stuik, R., Jolissaint, L., Kendrew, S., et al. 2010, Proc. SPIE, 7736, 77363G
Thomas, S. J., Soummer, R., Dillon, D., et al. 2011, AJ, 142, 119